Physico-chemical principles of AC electrosynthesis: reversible reactions

Yong Rui Poh,[1] Yu Kawamata,[2] and Joel Yuen-Zhou[1,*]

[1] *Department of Chemistry and Biochemistry, University of California San Diego, La Jolla, California 92093, USA*
[2] *Department of Chemistry, Scripps Research, La Jolla, CA 92037, USA*

(Dated: July 25, 2024)

Electrolysis integrates renewable energy into chemical manufacturing and is key towards sustainable chemistry. Controlling the waveform beyond direct current (DC) addresses the long-standing obstacle of chemoselectivity, yet it also expands the parameter set to optimise, creating a demand for theoretical predictions. Here, we report the first analytical theory for predicting chemoselectivity in alternating current (AC) electrosynthesis. The mechanism is a selective reversal of the unwanted redox reaction during periods of opposite polarity, reflected in the final reaction outcome as a time-averaged effect. In the ideal scenario of all redox reactions being reversible, square AC waveform biases the outcome towards more overoxidation/overreduction, whereas sine AC waveform exhibits the opposite effect. However, in a more realistic scenario of some redox reactions being quasi-reversible, sine AC may behave mostly like square AC. These predictions are in numerical agreement with model experiments employing acetophenone and align qualitatively with literature precedent. Collectively, this study provides theoretical proof for a growing trend that promotes changing waveform to overcome limitations challenging to address by varying canonical electrochemical parameters.

INTRODUCTION

Electrosynthesis is enjoying a renaissance as a sustainable and enabling way to drive chemical reactions [1–6]. While electrochemical transformations using direct current (DC) – including constant current and constant potential methods – are well-developed [7–10], considerably less effort has been made with alternating current (AC), whereby electrons reverse their flow periodically [11–14]. The latter has the advantage of introducing additional controllable parameters such as oscillation frequency and waveform shape, creating more opportunities for reaction control [15–21]. In particular, this has been useful in minimising loss of electrocatalysts [22–27], achieving paired electrosynthesis [24, 28–32], and improving chemical selectivity [26, 29, 33–44]. These benefits are also transferrable to the manufacturing industry – recently, Hioki et al. used AC to upgrade biomass-derived carboxylic acids into valuable polymers [41], setting yet another milestone in green engineering.

As expected, having more parameters also complicates the reaction optimisation process, a growing concern with AC electrolysis [15, 19]. These problems may be alleviated with theoretical models – for instance, Blanco et al. trained a neural network with small-scale optimisation data to artificially explore a broader range of synthetic conditions [34]. Another approach is to establish first-principles theories that are predictive for general reaction schemes without the need for prior experimentation. However, most of these frameworks have been developed for electroanalysis [45–51] and hence are not directly applicable to the present context of bulk electrolysis. Pioneering computational and experimental studies were made by Fedkiw and co-workers between 1984 and 1993 [52–56], where they modelled electrochemical reactions as sequences of irreversible steps. The reaction outcome in these early explorations was highly sensitive to the reaction and AC parameters with no definitive qualitative trends identified. Assumptions of reaction irreversibility played an important role in these studies, bypassing the consideration of reversible electron transfers mediated by alternating polarity (even if the overall reaction were to be irreversible or quasi-reversible) [39, 40, 44, 57].

In contrast to these prior studies, we consider a minimal model that treats electron transfers as fast reversible processes, establishing the first analytical theory for AC-driven chemoselectivity control over simple branched reaction schemes [Fig. 1]. The analytical results are amenable to simple qualitative interpretations and we find the reaction yield to be dependent on the diffusion dynamics (i.e. current) near the electrode surface. Under most experimental AC conditions, the rapidly-oscillating reaction dynamics are realised in the long run as a time-averaging (coarse-graining) effect of nonequilibrium diffusive fluxes, which sometimes has no equilibrium analogue. As such, different waveforms will lead to differently-averaged reaction behaviours and hence different chemoselectivities. In particular, when products are formed with 1:1 stoichiometry, switching from DC to square waves (also termed rapid alternating polarity or rAP) can completely invert chemoselectivity control towards the pathway involving more electrons, facilitating over-oxidation/over-reduction. By contrast, sinusoidal waves exhibit the opposite trend of favouring less-oxidised/less-reduced products [Fig. 1A]. Mechanistically, in terms of diffusive fluxes (or currents), square AC causes a selective reverse reduction/oxidation of the less-oxidised/less-reduced product (and vice versa for sine AC), a possibility proposed experimentally by Rodrigo et al. [44]. As for branched reactions transferring the same number of electrons but with different product stoichiometries, square (sine) AC favours pathways containing fewer (more) products [Fig. 1B]. Notably, the model predictions are confirmed quantitatively through experimental observation of acetophenone reduction, a reaction that represents the more general case of products differing in both oxidation state (number of electrons transferred) and product stoichiometry [Fig. 1C]. Furthermore, qualitative agreement is possible with multiple experimental works in the literature [29, 34, 37, 39, 40]. These suggest that our minimal model may have captured the important dynamics in AC electrosynthesis, thereby concluding AC modulation to be a promising solution to chemoselectivity issues when the reaction cannot be optimised by tweaking conventional electrochemical parameters. While we have not considered elements such as galvanostatic control and follow-up chemical steps from products of either/both electrodes, our model can be extended into this more general form and such efforts are underway.

* joelyuen@ucsd.edu

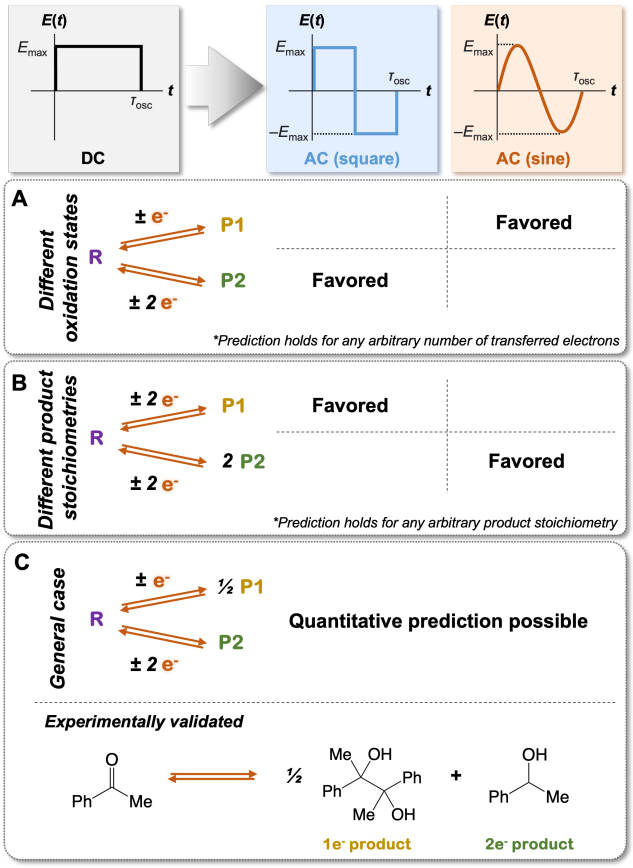

FIG. 1: Theoretical proof for AC-driven chemoselectivity. In this work, we present theoretical evidence for a growing set of experimental observations that propose control over electrochemical chemoselectivity by changing waveforms. The predictions are as followed: (**A**) Between two pathways transferring different number of electrons, square (sine) AC favours the route that transfers more (fewer) electrons. An example for one versus two electrons has been shown. (**B**) Between two pathways resulting in products of different stoichiometries, square (sine) AC favours the route with lower (higher) stoichiometry. An example for one vs two product molecules has been shown. (**C**) A general reaction can branch into products differing in both oxidation state and stoichiometry. In that case, quantitative prediction is possible. This was achieved experimentally by this work using acetophenone reduction as an example. See also Table 1.

RESULTS AND DISCUSSION

Theoretical framework

Our model comprises a single reductant (Re) being oxidised at the double layer of a planar anode (the same results may be obtained with cathodic reactions) [Fig. 2A]. We assume the cathode to be "far away enough" such that it can be ignored; we will quantify this statement later. In contrast with Fedkiw and their colleagues [52–56], we consider all electron-transfer kinetics to be faster than mass transport and polarity changes due to AC. As such, we assume electrochemical equilibrium at the double layer at all times with concentrations obeying the Nernst equation. While this implies a reversible electrochemical reaction, we expect the same outcome in quasi-reversible processes as well (i.e. processes with slow electron transfers before a threshold potential), in which case reverse product oxidation can occur either through potential cycling by AC or at the anode of an undivided cell (made possible by convection from stirring or migration during the long reaction time of bulk electrolysis) [Fig. 2A]. More about the implications of deviating from reversibility will be discussed later. We further assume chemical equilibria in all non-electrolytic reactions; this makes our theory agnostic to the reaction mechanism, that is, the only chemical species to consider are stable species that approach or leave the anode. To introduce chemoselectivity, we consider two possible oxidants, $(\mathrm{Ox}, 1)$ and $(\mathrm{Ox}, 2)$, leaving the anode, with the overall reaction scheme being

$$m_2\,(\mathrm{Ox}, 2) + n_2 e \rightleftharpoons \mathrm{Re} \rightleftharpoons m_1\,(\mathrm{Ox}, 1) + n_1 e, \qquad (1)$$

where formal charges have been omitted for simplicity. Finally, we assume that electron transfer only occurs when the redox-active species approach the anode, which we assume to be dominated by Fickian diffusion. Overall, the reaction yield and chemoselectivity being studied is an interplay between the equilibrium concentrations of reactant and product species at the electrode and their non-equilibrium mass transport away from the electrode, which will converge to an equilibrium outcome being observed in the bulk after a long reaction time.

We solve the diffusion kinetics analytically starting from the following parameters: $c^*_{\mathrm{Ox},2}$ = initial $(\mathrm{Ox}, 2)$ concentration, c^*_{Re} = initial Re concentration, $D_{\mathrm{Ox},\xi}/D_{\mathrm{Re}}$ = ratio of (Ox, ξ) diffusion constant to Re diffusion constant ($\xi \in \{1, 2\}$), $E^{\mathrm{o}}_1 - E^{\mathrm{o}}_2$ = difference in standard reduction potentials of $(\mathrm{Ox}, 1)$ and $(\mathrm{Ox}, 2)$ [58], T_{r} = reaction time, and T = temperature. Also used are the gas constant R and the Faraday constant F. Due to the assumption of electrochemical equilibria, these parameters determine the initial $(\mathrm{Ox}, 1)$ concentration $c^*_{\mathrm{Ox},1}$ through the Nernst equation. In addition, we consider direct control of the anodic potential via three different time-profiles $E\,(t)$ [59]: DC, square AC and sinusoidal AC. While we assume $E\,(0) = 0$, effects of constant bias to the applied voltage can be understood with our model by an effective shift in the E^{o}_ξ value. Comparisons between different waveforms are made by keeping the amplitude (peak voltage) $E_{\max}$ constant [Fig. 2B]. In cases of AC, we ignore effects due to double layer charging/discharging, valid if the oscillation period τ_{osc} is longer than tens of milliseconds [60]. After solving for the concentration time-profiles at the double layer $c^{\mathrm{DL}}_j\,(t)$ ($j \in \{\mathrm{Re}, (\mathrm{Ox}, 1), (\mathrm{Ox}, 2)\}$), we quantify the reaction yield Y_ξ of product (Ox, ξ) by counting (integrating) the amount of products diffusing away from the anode during the reaction time (i.e. the double-layer flux or current) and dividing the result by the stoichiometric number m_ξ and the initial reactant amount Vc^*_{Re} (V = electrolytic cell volume). From here, we measure chemoselectivity using the branching ratio $\theta \equiv Y_2/Y_1$, defined as the ratio of reaction yields (see Supplementary Information S1 and S2, particularly Eqs. (S6) and (S15)).

Controlling pathways with different changes in oxidation state

When both reactions have equal product stoichiometries ($m_1 = m_2$), we find the square waveform to favour the reaction with more electrons, i.e. the more-oxidised product, across all $E_{\max}$ values when compared to DC. By contrast, sinusoidal waves favour processes transferring fewer electrons (the less-oxidised product). This shows that waveform control can not only bias a particular reaction pathway but also modulate the direction of this bias. An example with $n_1 = 1$ and $n_2 = 2$ (i.e. $(\mathrm{Ox}, 2)$ being the more-oxidised

product) has been shown in Fig. 3A. These findings can be rationalised by plotting reaction yields against E_{max} [Fig. 3B-C], which shows that reversing the polarity through the square waveform reduces the yield of the less-oxidised product more significantly than its more-oxidised counterpart (e.g. $Y_1^{square}/Y_1^{DC} = 0.52$ versus $Y_2^{square}/Y_2^{DC} = 0.55$ at $E_{max} = 0.30$ V). Thus, backward reduction of the less-oxidised species is the likely explanation for the above observations; this analysis aligns with the hypothesis proposed by Rodrigo et al. [44]. To investigate this further, we increase the initial concentration of the less-oxidised species by changing $E_1^o - E_2^o$, which shifts the initial equilibrium position [61]. This leads to enhanced control over reaction pathways by AC [Fig. 3D], supporting our hypothesis that a backward reduction is at play. Strikingly, we find a region of E_{max} in which a square wave can completely reverse the chemoselectivity by moving θ from < 1 in DC (under-oxidation) to > 1 (over-oxidation); the same is true for sinusoidal waveforms but for the converse effect. At this new $E_1^o - E_2^o$ value, we also screen the initial concentration of the less-oxidised species (which then determines the initial concentration of the more-oxidised species). The aforementioned E_{max} region changes as well [Fig. 3E], which suggests that spiking the reaction mixture with products can modulate the reaction outcome.

We note that chemoselectivity can also be controlled by directly changing E_{max} under DC conditions; in this case, the branching ratio increases with E_{max} [Fig. 3A]. However, this option is not always feasible due to other considerations like longer reaction times or competition from other redox pathways [60]. Also, throughout this work, we keep $D_{Ox,1} = D_{Ox,2} = D_{Re}$, which is approximately true lest major changes to the formal charge or molecule size after the redox transformation [60].

Mechanistic investigations

To further confirm the mechanism of selectivity control, we begin with the general expression of Y_ξ given by Eq. (S12) and derive an approximate expression for Y_ξ, valid after many AC oscillations (see Supplementary Information S2). It reads

$$Y_\xi \approx \frac{\int_0^{\tau_{osc}} dt\ \left[c_{Ox,\xi}^{DL}(t) - c_{Ox,\xi}^*\right]}{\tau_{osc}} \times A\sqrt{\frac{4D_{Ox,\xi}T_r}{\pi}} \times \frac{1}{Vc_{Re}^* m_\xi}, \tag{2}$$

where A is the electrode surface area. Eq. (2) has a simple interpretation: In order of appearance, it is the concentration gradient between the double layer and the bulk (which, being far away from the electrode, has a concentration close to the initial value), averaged over one oscillation period τ_{osc}, multiplied by the characteristic diffusion volume, and divided by the initial reactant quantity. Physically, this implies that the rapidly-oscillating diffusion dynamics (mass transport), represented by the concentration gradient through Fick's first law, may be ironed out by running the reaction for a long time such that the observed reaction outcome is "coarse-grained" [Fig. 4A]. Therefore, different waveforms can result in differently-averaged diffusion behaviours and different reaction selectivities. We emphasise that the time-averaged result above may only be realised in an experimental setting if the oscillation period is also much shorter than the time required to equilibrate throughout the electrochemical cell. Otherwise, the reaction outcome should naturally simplify to that of an equilibrated DC electrolysis dictated by the final potential. Since our model does not account for finite-size effects of the electrochemical cell, the onset of this latter regime cannot be explicitly captured by our present model. As an aside, when we assumed a "far-away-enough" cathode, we meant a cathode-anode distance that is much larger than the distance diffused within a single AC oscillation. This is also the experimentally-relevant case.

The reaction selectivity is quantified by the branching ratio θ, which is a fraction of reaction yields [Eq. (2)]:

$$\theta \equiv \frac{Y_2}{Y_1} \approx \frac{\int_0^{\tau_{osc}} dt\ \left[c_{Ox,2}^{DL}(t) - c_{Ox,2}^*\right]}{\int_0^{\tau_{osc}} dt\ \left[c_{Ox,1}^{DL}(t) - c_{Ox,1}^*\right]} \sqrt{\frac{D_{Ox,2}}{D_{Ox,1}}} \frac{m_1}{m_2}. \tag{3}$$

To further simplify Eq. (3), we consider the case of $m_1 = m_2 = 1$ and substitute the Nernst equation of $c_{Ox,\xi}^{DL}(t) = c_{Re}^{DL}(t)\, e^{n_\xi F\left[E(t) - E_\xi^o\right]/RT}$ (note that $E(0) = 0$). Then, by assuming $c_{Re}^{DL}(t) \approx c_{Re}^*$ within a short time period of $0 \le t \le \tau_{osc}$ (valid if the reaction proceeds to a small extent during each oscillation; see Supplementary Information S3), we obtain the simpler expression of

$$\theta \approx \frac{\int_0^{\tau_{osc}} dt\ \{[C(t)]^{n_2} - 1\}}{\int_0^{\tau_{osc}} dt\ \{[C(t)]^{n_1} - 1\}} P, \tag{4}$$

with $C(t) - 1 \equiv e^{FE(t)/RT} - 1$ representing the characteristic concentration gradient at time t and $P \equiv \left(c_{Ox,2}^*/c_{Ox,1}^*\right)\sqrt{D_{Ox,2}/D_{Ox,1}}$ being a proportionality constant unimportant to the overall trend. Note that although all plotted results correspond to Eq. (3) rather than Eq. (4), the latter allows for simple back-of-the-envelope estimates of chemoselectivity and forms the key qualitative result of this work [Fig. 4B]. For instance, a DC experiment will have $C(t) = C_{max} \equiv e^{FE_{max}/RT}$ at all times t. From here, the time-averaging integral easily computes out to be, using $n_1 = 1$ and $n_2 = 2$ as an example,

$$\theta_{DC} \approx \frac{C_{max}^2 - 1}{C_{max} - 1} P. \tag{5}$$

For a specific case of $E_{max} = (RT/F)\ln 2$ or $C_{max} = 2$, θ_{DC} is approximately $3P$. Larger E_{max} values will result in higher C_{max} values, which translates as steeper concentration gradients for the over-oxidation pathway and higher θ values. This is in line with Fig. 3A and is expected from observing the Nernst equation [60].

To understand the effect of waveform control, we consider a square wave experiment conducted with the same E_{max} value of $(RT/F)\ln 2$. This means $C(t) = C_{max}$ during the first half of the oscillation period and $C(t) = e^{-FE_{max}/RT} = 1/C_{max}$ during the second half (when the polarity is reversed). Partitioning the time integrals of Eq. (4) into halves (i.e. $\int_0^{\tau_{osc}} dt = \int_0^{\tau_{osc}/2} dt + \int_{\tau_{osc}/2}^{\tau_{osc}} dt$) yields

$$\theta_{square} \approx \frac{\left(C_{max}^2 - 1\right)/2 + \left(1/C_{max}^2 - 1\right)/2}{\left(C_{max} - 1\right)/2 + \left(1/C_{max} - 1\right)/2} P \tag{6}$$

$$= \frac{C_{max}^2 + 1/C_{max}^2 - 2}{C_{max} + 1/C_{max} - 2} P, \tag{7}$$

which, using the first expression, equals $(1.500 - 0.375)/(0.500 - 0.250) \times P$ when $C_{max} = 2$. Because the values -0.250 and -0.375 are negative, they indicate negative concentration gradients and hence backward reductions of processes 1 and 2 during times of opposite polarity. Despite this being more significant in the process that transfers more electrons (process 2 in the above example), its degree of backward reduction *relative* to that of forward oxidation is *smaller* than its counterpart of fewer electrons ($0.375/1.500$ is smaller than $0.250/0.500$). Thus, overall, the less-oxidised species is selectively reduced to Re, then converted to the more-oxidised product through

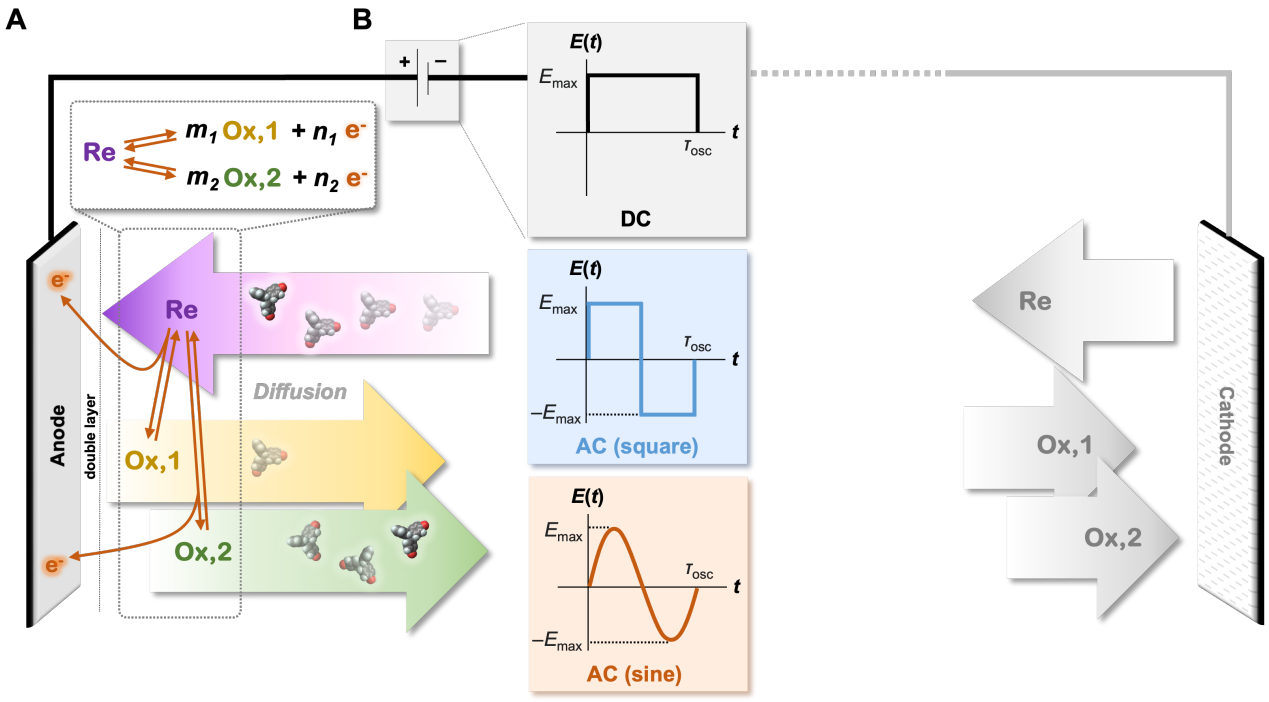

FIG. 2: **Modelling AC-induced chemoselectivity.** (**A**) Diagrammatic representation of the theoretical model. We consider a branched electrochemical reaction occuring quickly at the electrode surface, with the overall reaction rate being determined by diffusive flux near the electrode surface (i.e. current). Also shown are products being reversed to the reactant at the counter electrode. This will occur experimentally in an undivided cell and allows our model on reversible processes at the working electrode to be extended to quasi-reversible reactions at both electrodes. (**B**) Shapes of potential waveform being considered in this work. Changing the waveform has implications on the branching ratio between the two products.

temporal control of concentration gradients, biasing the over-oxidation pathways and confirming our earlier hypothesis about the mechanism of chemoselectivity. Indeed, θ_{square} computes as $\approx 4.5P$, which is larger than the DC result of $\approx 3P$ [Fig. 4B]. A similar analysis done for sinusoidal AC reveals $\theta_{\text{sine}} < \theta_{\text{DC}}$. Interestingly, under most experimental conditions, the amount of product depleted due to sinusoidal waveforms is negligible compared to the amount of product formed (see Supplementary Information S4), thus the bias towards less-oxidised/less-reduced pathways occurs mostly due to the lower voltage of sine AC as compared to DC over every oscillation (see, for instance, Fig. 3A). This also implies that a non-negative sinusoidal wave, such as $E(t) = E_{\text{max}} |\sin(2\pi t/\tau_{\text{osc}})|$, will not change the branching ratio by much compared to regular sine AC, consistent with the simulation results [Fig. S1]. Ultimately, this highlights the importance of the waveform chosen to selectively remove side-products.

Controlling pathways of different product stoichiometries

For branched reactions of different product stoichiometries ($m_1 \neq m_2$), we expect square (sine) waves to favour processes containing fewer (more) products, more so than DC does. This is because the Nernst equation yields $c^{\text{DL}}_{\text{Ox},\xi}(t) \sim [C(t)]^{n_\xi/m_\xi}$, that is, increasing m_ξ should have an opposite effect on the concentration gradient as compared to increasing n_ξ. Indeed, we observe this relationship in Fig. 5A-C with $m_1 = 1$ and $m_2 = 0.5$ (keeping $n_1 = n_2 = 1$), albeit tiny in the square AC case. Interestingly, θ is mostly independent of E_{max} at large values of E_{max}, in contrast with the case of different product oxidation states [Fig. 3A]. Examining approximate expressions for θ reveals a lack of dependence of θ on $E(t)$ – apart from its sign – when the magnitude of $E(t)$ is large, consistent with the above observations. The reversed selectivity created by square AC is attributed to the same mechanism of backward reduction (Supplementary Information S5). Again, a non-negative sinusoidal wave, such as $E(t) = E_{\text{max}} |\sin(2\pi t/\tau_{\text{osc}})|$, does not change the branching ratio by much compared to regular sine AC [Fig. S2], which is consistent with our earlier discussion about how the primary role of sine AC is to offer a lower voltage than DC.

As a final demonstration of AC-induced chemoselectivity, we increase the initial concentration of the higher-stoichiometry product to be comparable to the initial reactant concentration. This way, backward reduction of this product can occur to an appreciable extent when the polarity is reversed in AC. Indeed, the product of higher stoichiometry is depleted under both square and sinusoidal waves, offering a branching ratio of infinity [Fig. 5D-E]. This represents the epitome of selectivity control – we can now convert side products to the desired compound using AC. Alternatively, if we consider this product as the reactant instead, then our model can also be extended to AC-driven paired electrolysis [15–17, 19]. While the conversion ratio is low at the moment, we expect to obtain better results once the waveform has been optimised. Works in this direction are ongoing.

General observations about AC-driven chemoselectivity

The expression for θ in Eq. (3) reveals a few general conclusions about waveform-induced chemoselectivity. Because Eq. (3) is independent of AC period and reaction

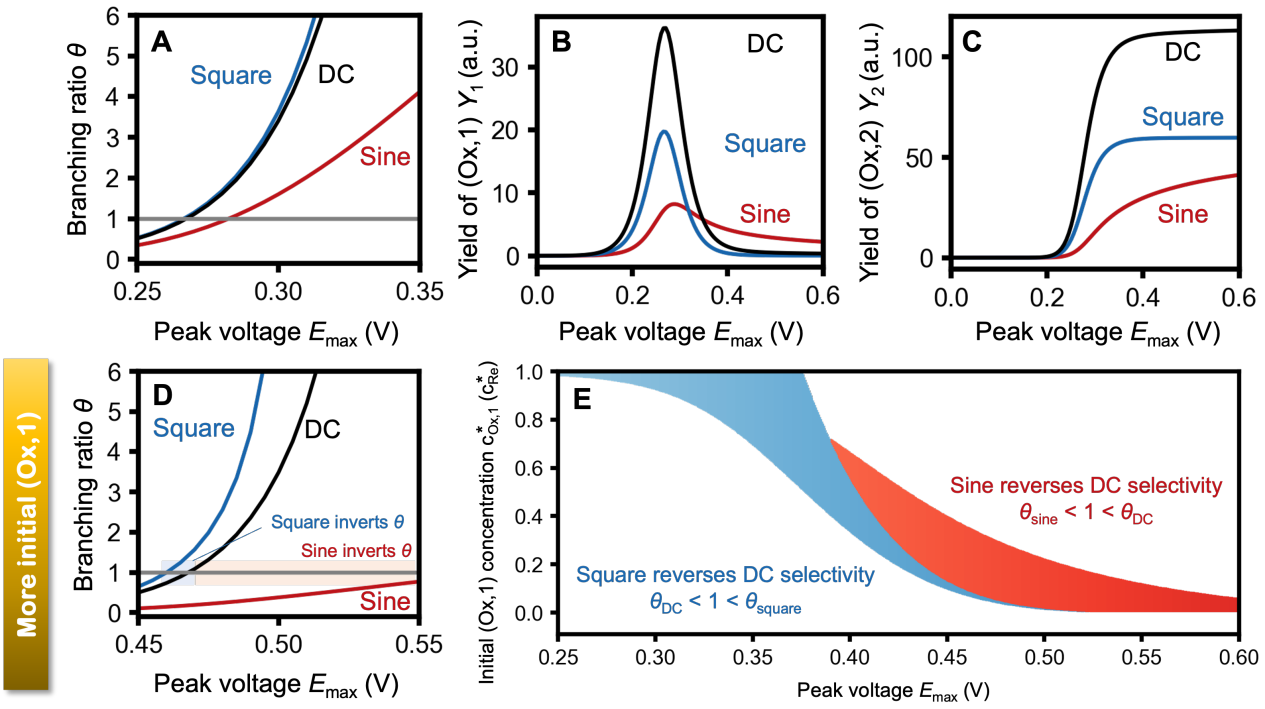

FIG. 3: **Controlling pathways with different changes in oxidation state using AC.** (**A**) Branching ratios (θ) at different peak voltages ($E_{\max}$) for various waveform shapes of the same amplitude. Larger θ indicates higher production of the more-oxidised product over the less-oxidised one. (**B**) Yields of the less-oxidised product (Y_1). The values at $E_{\max} = 0.30$ V are 23.3 (DC), 12.1 (square) and 8.0 (sine). (**C**) Yields of the more-oxidised product (Y_2). The values at $E_{\max} = 0.30$ V are 79.5 (DC), 43.8 (square) and 12.8 (sine). (**D**) Branching ratios when the initial concentration of the less-oxidised product is increased. Square AC inverts θ relative to DC at $E_{\max} \approx 0.46$ V. (**E**) Regions of $E_{\max}$ within which square AC changes θ from < 1 in DC (under-oxidation) to > 1 (over-oxidation), plotted across different initial product concentrations. Also shown are $E_{\max}$ regions in which sinusoidal AC changes θ from > 1 in DC to < 1. (Parameters: $n_1 = 1$, $n_2 = 2$, $m_1 = m_2 = 1$, $D_{\mathrm{Ox},1} = D_{\mathrm{Ox},2} = D_{\mathrm{Re}}$, $\tau_{\mathrm{osc}} = 1/60$ s, $T_{\mathrm{r}} = 1$ hour and $T = 25\,^{\circ}$C. For (**A**-**C**), $E_1^{\circ} = E_2^{\circ}$ and $c^*_{\mathrm{Ox},2} = 1.0 \times 10^{-9} c^*_{\mathrm{Re}}$, which implies that $c^*_{\mathrm{Ox},1} = 3.2 \times 10^{-5} c^*_{\mathrm{Re}}$. For (**D**), $E_1^{\circ} - E_2^{\circ} = -0.20$ V and $c^*_{\mathrm{Ox},2} = 1.0 \times 10^{-9} c^*_{\mathrm{Re}}$, which implies that $c^*_{\mathrm{Ox},1} = 7.6 \times 10^{-2} c^*_{\mathrm{Re}}$. For (**E**), $E_1^{\circ} - E_2^{\circ} = -0.20$ V. Note that here the choice of $c^*_{\mathrm{Ox},1}$ determines the value of $c^*_{\mathrm{Ox},2}$. All reaction yields are plotted relative to $(A/V)\sqrt{D_j/\pi}$ with units of $\mathrm{s}^{1/2}$; j indexes the product.)

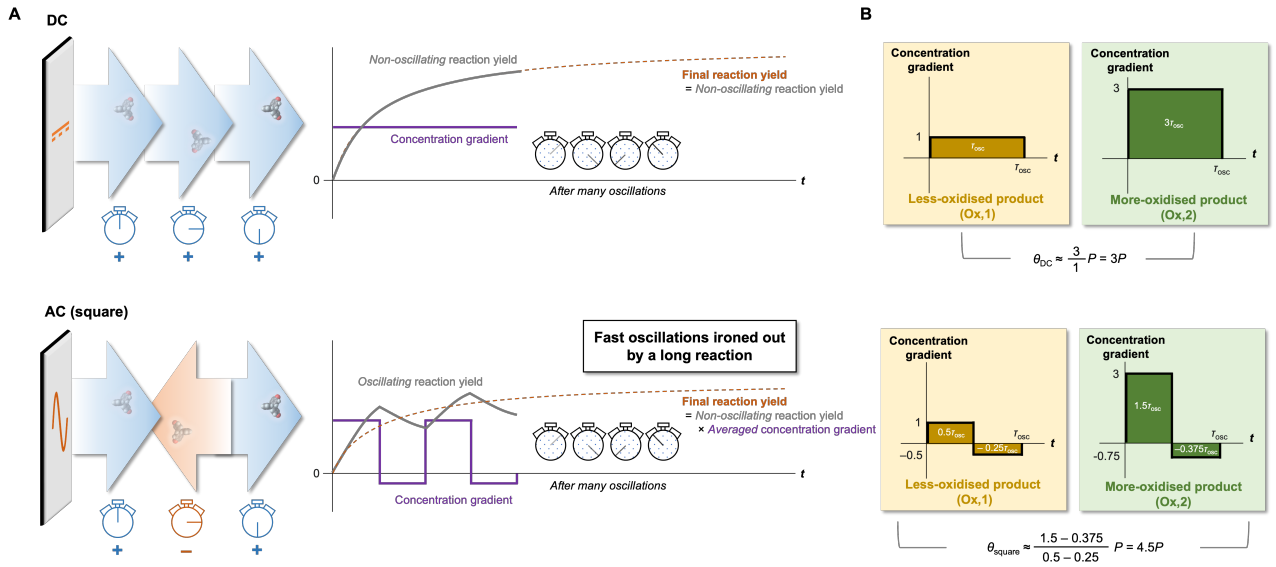

FIG. 4: **Mechanism behind AC-driven chemoselectivity.** (**A**) Interpreting the approximate expression for reaction yield (Y_ξ) [Eq. (2)] and visualisation of the time-averaging effect after a long AC reaction. (**B**) Back-of-the-envelope estimates of branching ratio (θ) using Eq. (4). When the polarity is reversed in a square AC experiment, the less-oxidised/less-reduced product is depleted more than the more-oxidised/more-reduced product relative to the amount formed during the forward process. Therefore, overall, square waveforms promote over-oxidation/over-reduction more so than DC does. (Parameters: $n_1 = 1$, $n_2 = 2$, $m_1 = m_2 = 1$, and $C_{\max} = 2$, which is equivalent to a peak voltage $E_{\max}$ of $(RT/F)\ln 2$.)

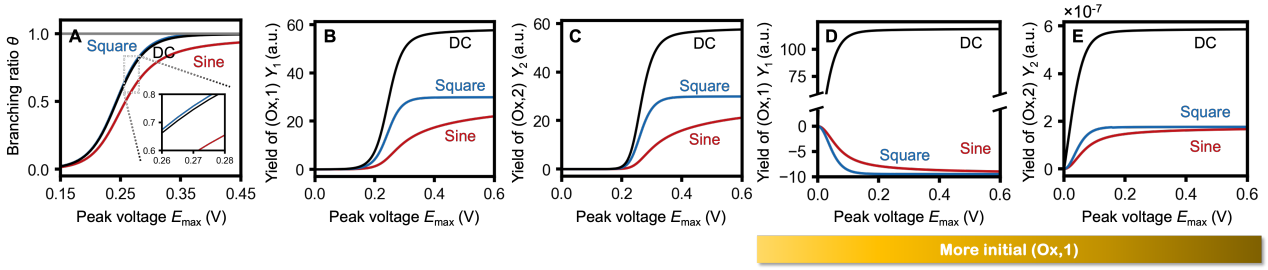

FIG. 5: **Controlling pathways with different product stoichiometries using AC.** (**A-C**) Branching ratios (θ) and yields (Y_1, Y_2) at different peak voltages ($E_{\max}$) for various waveform shapes of the same amplitude. Larger θ indicates higher yield of the product with lower stoichiometry. Y_1 (Y_2) = yield of product with higher (lower) stoichiometry. Inset of (**A**): Same plot enlarged for 0.26 V $< E_{\max} <$ 0.28 V. (**D-E**) Yields when the initial concentration of the higher-stoichiometry product is increased and made comparable to the initial reactant concentration. Under these conditions, AC converts the product with higher stoichiometry to that with lower stoichiometry, demonstrating the pinnacle of chemoselectivity control. (Parameters: $n_1 = n_2 = 1$, $m_1 = 1$, $m_2 = 0.5$, $D_{\mathrm{Ox},1} = D_{\mathrm{Ox},2} = D_{\mathrm{Re}}$, $\tau_{\mathrm{osc}} = 1/60$ s, $T_{\mathrm{r}} = 1$ hour, $T = 25\,^{\circ}$C, $c^*_{\mathrm{Ox},2} = 1.0 \times 10^{-9} c^*_{\mathrm{Re}}$ and $c^*_{\mathrm{Re}} = 1$ M. For (**A-C**), $E^{\circ}_1 = E^{\circ}_2$, which implies that $c^*_{\mathrm{Ox},1} = 3.2 \times 10^{-5} c^*_{\mathrm{Re}}$. For (**D-E**), $E^{\circ}_1 - E^{\circ}_2 = -0.27$ V, which implies that $c^*_{\mathrm{Ox},1} = 1.2 c^*_{\mathrm{Re}}$. All reaction yields are plotted relative to $(A/V)\sqrt{D_j/\pi}$ with units of $\mathrm{s}^{1/2}$; j indexes the product.)

time after many AC oscillations (i.e. if the AC period is much shorter than the time needed to equilibrate the electrolytic cell; see Supplementary Information S6), optimisation of these parameters may be secondary to others when designing the reaction protocol. Also, because Eq. (3) relies only on the time-averaged dynamics within a single oscillation period, convection is unlikely to change the predictions if the reaction continues to take a long time before equilibrating throughout the electrochemical cell. This is true for many stirred reactions, which require hours to complete (whereas AC oscillations can occur within seconds [60]). Interestingly, under an AC potential, the reaction outcome carries some information about the trajectory towards this state as a time-averaged effect. This offers an avenue for detecting synchronous processes that occur within an oscillation period, such as other non-electrochemical follow-up reactions.

The chemoselectivity trends discussed in this work are summarised in Table 1.

Limitations of the theoretical analysis

In using a model minimal enough to admit an analytical solution, we acknowledge two main assumptions that are not fully representative of most AC electrosynthetic experiments. We do not expect these assumptions to have a huge impact on the general conclusions made by this work.

The first major assumption is that of fast, reversible electrode kinetics that creates a Nernstian equilibrium at the electrode surface. Indeed, it is known that most electrochemical reactions exhibit *relatively* sluggish electrode kinetics and are hence classified as either quasi-reversible or irreversible [57]. However, it is important to note that this classification is based solely on the experimentally-recorded cyclic voltammogram, that is, the electron transfer and/or other follow-up chemical reactions were slow relative to the time needed to traverse the cyclic voltammetric wave (which is typically a few seconds) and so "irreversibility" was observed (see, for instance, Chapter 7 of Ref. [60]). Therefore, by the above definition of "irreversibility", we expect our model to be the most accurate for AC oscillations that occur slowly enough (perhaps tens of seconds but definitely system-dependent) such that the reaction kinetics is fast and approaches the reversible limit *from the perspective of the AC*. Beyond this regime, we can make the following qualitative statements:

1. We note that our observable of interest is the branching ratio after the reaction has completed, which takes hours and is usually the longest timescale of any electrosynthetic experiment. From this perspective, we conjecture that most electrochemical reactions are "reversible", with any deviation from "reversibility" being smeared out by the long reaction time relative to the oscillation period and reaction rates. Thus, we expect the chemoselectivity *trends*, as described by Table 1, to remain unchanged for quasi-reversible or irreversible systems (following electrochemical definitions) unless the kinetic barrier to the reverse reaction is extremely high, such as in gas evolution reactions (in which case the system's longest timescale becomes the return of the evolved gas back into the reactor). Note that quantitative proof of this statement is still in the works.

2. Even though the *trends* may remain unchanged, we expect the *degree* of selectivity bias to differ from the present predictions. As mentioned, the rates of synchronous processes such as electron transfer and/or any slow follow-up chemical steps may offer an additional timescale against which the AC frequency may be optimised for the best chemoselectivity. This has been experimentally observed [29, 39] and theoretical developments in this direction are ongoing. We expect the analysis to be similar to how AC cyclic voltammetry offers information about electron transfer and follow-up chemical rate constants [60, 62]. Closely related is the theory of catalytic resonance, where surface-catalysed reactions are accelerated by oscillating or pulsing the catalytic activity at a frequency close to each individual rate in the adsorption-reaction-desorption chemical network (the so-called "resonance" effect) [63–72]. This idea, pioneered by Dauenhauer, also falls into the bigger picture of molecular ratcheting [73, 74].

The second major assumption is that of fast double-layer charging/discharging relative to the AC oscillation period. To quantify this statement, we note that most AC electrosynthesis experiments are conducted using two-electrode cells with a solution resistance of around 100 Ω and a double-layer capacitance of around 1 mF. This places the charging timescale at around 0.1 s from a simple RC-circuit consideration [32, 37, 67]. Thus, our model's assumption is valid

under AC frequencies of $\lesssim 10$ Hz, which is the typical experimental frequency. Above this AC frequency, much of each AC oscillation (and hence the reaction time) is spent rearranging the double layer, the dynamics of which can have microscopic impacts on the branching ratios. For instance, an unequilibrated, inhomogeneous double-layer structure generated by rapid AC oscillations has been reported to stabilise certain reactive intermediates through oscillating local electric field effects, thereby influencing the chemoselectivity [67, 75–79]. Incidentally, there exists also a minimum AC frequency for our model. As discussed before, if the molecules could diffuse across the container within an AC period, then the electrode surface will be in equilibrium with the bulk at most times and any non-equilibrium effects predicted by our model will be lost. For molecules of diffusion constants $10^{-6}\,\mathrm{cm^2\,s^{-1}}$ in small electrochemical reactors of 1 cm widths [60], the AC frequency needs to be $\gtrsim 10^{-6}$ Hz; this is met by most experimental set-ups.

Experimental validation with acetophenone reduction

We next verified our theoretical predictions using acetophenone reduction as a model reaction. Under both DC and AC electrolysis, acetophenone (**1**) was reduced to either 2,3-diphenyl-2,3-butanediols (**2a** and **2b**) through a one-electron dimerisation pathway or 1-methylbenzylalcohol (**3**) through a two-electron pathway [Fig. 6A]. Quasi-reversibility of all products was verified by cyclic voltammetry with both cathodic and anodic peaks being observed at a scan rate of $100\,\mathrm{mV\,s^{-1}}$ and with a peak separation of around 4 V (see Supplementary Information S8). We appreciate that there are different guidelines distinguishing between quasi-reversibility and irreversibility; here, we shall label an electrochemical reaction as quasi-reversible if its cyclic voltammogram displays both cathodic and anodic waves of the same redox couple heavily shifted relative to each other. As an aside, we note that our reduction products of interest are stable alcohols generated from protonating the unstable ketyl radical anion intermediate [80]. Because the reverse deprotonation is slow, the overall process is quasi-reversible; if, instead, the protonation step is eliminated by using a less acidic solvent like dimethylformamide with a high scan rate above $300\,\mathrm{mV\,s^{-1}}$, then the electron transfer can be electrochemically reversible [81].

The chemoselectivity studied in this reaction is slightly more complex than the simple cases discussed above, since it involves branching where both product stoichiometry and number of electrons are different. Nonetheless, our theory can be readily applied to provide some quantitative understanding of it. Strikingly, experimental branching ratios (**3** against **[2a**+**2b]**) of 0.02 under DC and 0.07 under square AC were reproduced numerically (0.03 and 0.07 respectively) using reasonable simulation parameters [Fig. 6B-E]. Furthermore, the experimentally-observed decrease in overall product yield when moving from DC to AC was captured by our model as a consequence of more-favourable **[2a**+**2b]** and **3** back-oxidations under AC waveforms. We note that being a quasi-reversible process, acetophenone reduction experiences kinetic limitations at the electrode surface, that is, there exists an effective threshold potential before the sluggish electron-transfer kinetics is lifted. This causes the sine waveform to appear similar to the square waveform for amplitudes close to the threshold potential, in which case we expect its product distribution to match the square AC predictions [Fig. 6F] (direct comparison to support this statement can be found in Fig. 1 of Ref. [41] and its Supporting Information also includes discussions on why sine AC is similar to square AC in terms of the reaction outcome). Indeed, the experimental branching ratio of 0.08 under sine AC was closer to the square waveform prediction (0.07) than the sine waveform result (0.02) [Fig. 6E]. All in all, the product distributions from experimental acetophenone electrolysis agree with and lend support to our theoretical model. Although here the impact of waveform change on the final product distribution was marginal, in general it is possible to experience a different, perhaps more dramatic (but also possibly diminished) effect in other systems, especially in the presence of more complex reaction networks incorporating multiple electron transfer and irreversible reaction steps. Notably, the difference in crude NMR yields of **3** among various waveforms is only around 1% [Fig. 6E], which may seem to leave some ambiguity in the experimental validation. For that reason, a simple statistical analysis is useful. Roughly speaking, if we assume every peak area integrated from the ^{1}H-NMR spectra to have a relative error of 40% (a conservative estimate compared to typical errors of $1-10\%$ [82, 83]), then we obtain $\theta_{\mathrm{DC}} = 0.017 \pm 0.010$ and $\theta_{\mathrm{square}} = 0.079 \pm 0.045$ (see Supplementary Information S9). In other words, the two branching ratios are well-separated in value within experimental uncertainty, with the largest value of θ_{DC} (at 0.027) being below the smallest value of θ_{square} (at 0.034). Nevertheless, efforts to find better examples complementing an improved model are ongoing.

Further comparison with published experimental data

To further demonstrate the reliability of our model, we performed a meta-analysis of experimental data from published results. For experimental works that fit categorically into our reaction scheme [39, 40], we find our predictions to agree qualitatively with the reported data. Both Gunasekera et al. [39] and Behera et al. [40] explored the oxidation of *N*-(4-methoxyphenyl)pyrrolidine tertiary amine at its α-carbon, where they found sinusoidal modulation of the applied voltage to minimise over-oxidation of the α-amino radical intermediate (the one-electron oxidation product) to the corresponding iminium cation (the two-electron oxidation product). This is in line with our predictions. Importantly, this allowed for further chemistry with the α-amino radical to obtain the desired product, which was an α-amino C–H arylation in Gunasekera et al. [39] and an α-amino C–H deuteration in Behera et al. [40]. Other validations of our theory were found in the same studies, where higher DC voltages exacerbated over-oxidation in Gunasekera et al. [39] and scanning the reaction yield across AC frequencies revealed flat regions of invariance in Behera et al. [40]. Strikingly, even for experiments that did not establish electrochemical (quasi-)reversibility [29, 34, 37], their results also confirm our predictions qualitatively. This is not surprising because an electrochemical process that displays irreversibility on its cyclic voltammogram can still be "reversible" under prolonged bulk electrolysis as speculated above. For instance, Kawamata et al. [37], who studied the competing reductions of a succinimide derivative to its two-electron hemiaminal product and four-electron lactam product, showed that potential-controlled sine and square ACs led solely to the less- and more-reduced products respectively, as opposed to DC where either the less-reduced product or a mixture was obtained, if any. In Blanco et al. [34], selectivity between the two-electron monomeric product, propionitrile, and the one-electron dimeric product, adiponitrile, during the reduction of acrylonitrile was found to be largely independent of AC frequency. As for the impact of waveform control, consistency is possible even though the analysis will be complicated by the two products differing in both oxidation states and product stoichiometries. Yet another confirmation is observed in Bortnikov et al. [29], where they found improvements in reaction yields of Ni-catalysed C–O cross-coupling when sine-wave potentials were utilised. This was because sinusoidal AC minimised

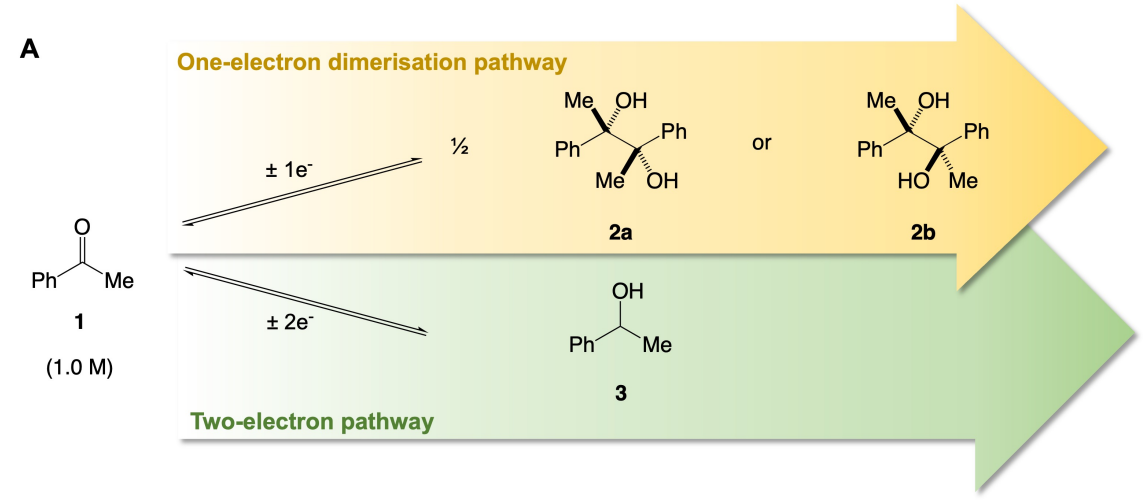

Conditions: tetrabutylammonium tetrafluoroborate (0.01 M), acetone/iPrOH (1/1, v/v), RVC/RVC, r.t., Ar atmosphere, 10 V, various waveforms (5 Hz if AC)

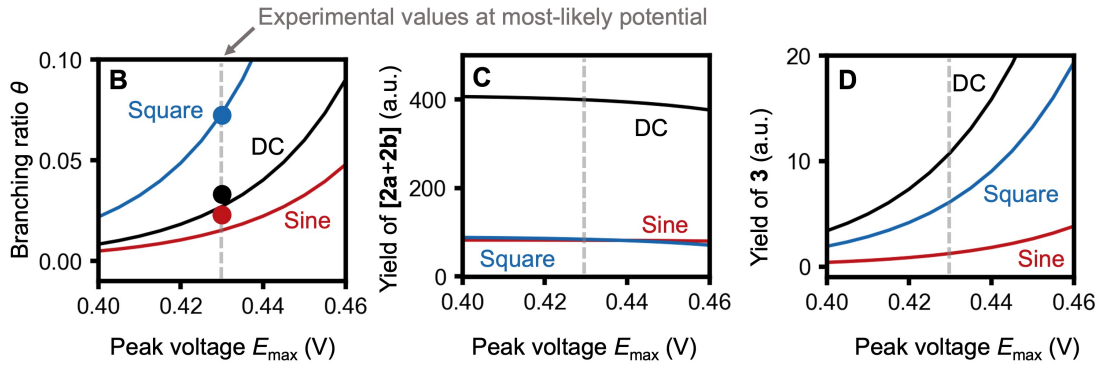

E

Waveform	Experimental		Simulated at E_{max} = 0.43 V
	% NMR yield (**1** : **[2a+2b]** : **3**)	Branching ratio (**3** / **[2a+2b]**)	Branching ratio (**3** / **[2a+2b]**)
DC	44% : 55% : 1%	0.02	0.03
Square	71% : 27% : 2%	0.07	0.07
Sine	86% : 13% : 1%	0.08	0.02

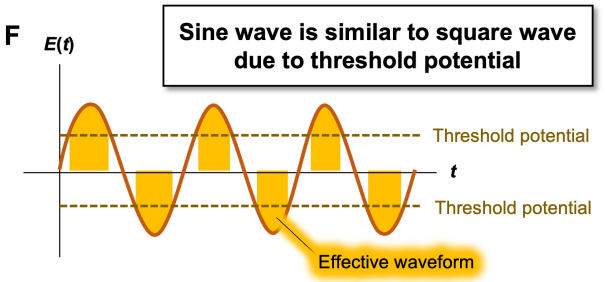

FIG. 6: **Experimental validation through acetophenone electrolysis.** (**A**) Products (**2a**, **2b**, and **3**) from reduction of acetophenone (**1**) under both potential-controlled DC and AC. These alcohols are formed with different oxidation states and stoichiometries and may be re-oxidised to acetophenone. (**B-D**) Predicted branching ratios (θ) and yields ($Y_{\mathbf{2a+2b}}$, $Y_{\mathbf{3}}$) at different peak voltages ($E_{\max}$) for various waveform shapes of the same amplitude. Larger θ indicates higher yield of **3**. Also plotted in solid dots are the experimental branching ratios. (**E**) Comparison between experimentally-measured (via crude NMR) and simulated branching ratios at $E_{\max} = 0.43$ V. (**F**) Effective waveform for sine AC due to sluggish electrode kinetics, that is, electron transfer only occurs past a threshold potential. (Simulation details: Numerical computation was performed assuming equal diffusivities for all compounds, 10^{-9} M (close to zero) initial concentration of **3**, and 0.25 V difference between the standard oxidation potentials of **[2a+2b]** and **3**, with the latter having the higher value. The computation was performed for a reaction time of 12 hours, although the branching ratio is independent of the reaction time at this limit [Eq. (3)]. Simulated reaction yields are plotted relative to $(A/V)\sqrt{D_j/\pi}$ with units of $s^{1/2}$; j indexes the product.)

unwanted reduction of the oxidative addition intermediate, which would otherwise have led to a second oxidative addition eventuating in the formation of undesired homocoupling products. Therefore, our study offers simple qualitative explanations by capturing only the key processes in AC electrosynthesis.

Given our pursuit for a minimal model, there are experiments of AC-induced selectivity that fall out of our model's scope. For instance, experiments that modulate the current (rather than the potential) [35–38, 41, 43] have not been considered yet. We note that such a protocol was recently used to elucidate the microscopic mechanism behind AC-induced chemoselectivity via a time-resolved operando electrochemical mass spectrometry platform capable of mapping out the kinetics of short-lived electrolytic intermediates [84]. Also, we have not considered reactions with important products at both electrodes, such as those concerning paired electrolysis and redox-neutral transformations [33, 37, 39, 44]. Notably, our model excludes slow electro- and non-electrochemical equilibria [29, 39, 40] and in some of these reactions the selectivity depended on an interplay between AC frequency and chemical kinetics [29, 39] as predicted earlier. Nevertheless, this study provides a framework for extensions towards such systems and works in these directions are ongoing.

CONCLUSION

By solving the diffusion dynamics for a branched reaction under AC potential control, we have developed a minimal model for understanding how waveform modulation can modify the product distribution of bulk electrosynthesis. Our analytical results suggest the cause to be a selective reversal of the unwanted product during times of reversed polarity, realised as a "coarse-grained" result after a long reaction. The model is applicable to many electrochemical reactions, including both anodic and cathodic processes and even cases of multiple reactant or product species in rapid chemical equilibria (such as the carboxyl acid-base pair in Hioki et al. [41]; see Supplementary Information S7). Moreover, it demonstrates how AC electrosynthesis can encode the path towards the steady state in the time-averaged outcome and may thus function as a probe for other concurrent processes such as millisecond chemical kinetics (analogous to analytical techniques such as AC cyclic voltammetry [60, 62] but applied to long-time reaction outcomes). As a testbed for our theory, we applied it to the reduction of acetophenone, successfully modeling the experimentally-obtained yields and branching ratios. A more qualitative comparison of our theory with other experiments in the literature also shows good agreement overall. Given the generality and simplicity of our results, we hope that this work will pave the way towards new chemoselective electrochemistry via waveform control. We expect AC electrosynthesis to be useful in situations where tuning other reaction parameters fails to achieve the desired result.

ACKNOWLEDGEMENTS

We thank Arghadip Koner, Nathan Romero, Roxanne Naumann, Andrew Pun, Joseph Derosa, Siyuan Su, and Long Luo for helpful discussions. Acknowledgment is made to the donors of The American Chemical Society Petroleum Research Fund for partial support of this research through the ACS PRF 60968-ND6 award.

[1] M. C. Bryan, P. J. Dunn, D. Entwistle, F. Gallou, S. G. Koenig, J. D. Hayler, M. R. Hickey, S. Hughes, M. E. Kopach, G. Moine, P. Richardson, F. Roschangar, A. Steven, and F. J. Weiberth, Green Chemistry **20**, 5082 (2018).
[2] Y. Yuan, J. Yang, and A. Lei, Chemical Society Reviews **50**, 10058 (2021).
[3] M. Munda, S. Niyogi, K. Shaw, S. Kundu, R. Nandi, and A. Bisai, Organic & Biomolecular Chemistry **20**, 727 (2022).
[4] J. Zhong, C. Ding, H. Kim, T. McCallum, and K. Ye, Green Synthesis and Catalysis **3**, 4 (2022).
[5] X. Cheng, A. Lei, T.-S. Mei, H.-C. Xu, K. Xu, and C. Zeng, CCS Chemistry **4**, 1120 (2022).
[6] Z. Yang, W. Shi, H. Alhumade, H. Yi, and A. Lei, Nature Synthesis **2**, 217 (2023).
[7] R. Francke and R. D. Little, Chemical Society Reviews **43**, 2492 (2014).
[8] S. R. Waldvogel and B. Janza, Angewandte Chemie International Edition **53**, 7122 (2014).
[9] M. Yan, Y. Kawamata, and P. S. Baran, Chemical Reviews **117**, 13230 (2017).
[10] M. Yan, Y. Kawamata, and P. S. Baran, Angewandte Chemie International Edition **57**, 4149 (2018).
[11] J. W. Shipley and M. T. Rogers, Canadian Journal of Research **17b**, 147 (1939).
[12] C. L. Wilson and W. T. Lippincott, Journal of The Electrochemical Society **103**, 672 (1956).
[13] R. C. Alkire and J. E. Tsai, Journal of The Electrochemical Society **129**, 1157 (1982).
[14] J. D. Lisius and P. W. Hart, Journal of The Electrochemical Society **138**, 3678 (1991).
[15] S. Rodrigo, D. Gunasekera, J. P. Mahajan, and L. Luo, Current Opinion in Electrochemistry **28**, 100712 (2021).
[16] M. Jamshidi, C. Fastie, and G. Hilt, Synthesis **54**, 4661 (2022).
[17] E. O. Bortnikov and S. N. Semenov, Current Opinion in Electrochemistry **35**, 101050 (2022).
[18] Y. Kawamata and P. S. Baran, J. Synth. Org. Chem., Jpn. **81**, 1020 (2023).
[19] L. Zeng, J. Wang, D. Wang, H. Yi, and A. Lei, Angewandte Chemie International Edition , e202309620 (2023).
[20] N. Behera, S. Rodrigo, A. Hazra, R. Maity, and L. Luo, Current Opinion in Electrochemistry **43**, 101439 (2024).
[21] A. P. Atkins and A. J. J. Lennox, Current Opinion in Electrochemistry , 101441 (2024).
[22] R. P. Wexler, P. Nuhant, T. J. Senter, and Z. J. Gale-Day, Organic Letters **21**, 4540 (2019).
[23] C. W. Lee, N. H. Cho, K. T. Nam, Y. J. Hwang, and B. K. Min, Nature Communications **10**, 3919 (2019).
[24] C. Schotten, C. J. Taylor, R. A. Bourne, T. W. Chamberlain, B. N. Nguyen, N. Kapur, and C. E. Willans, Reaction Chemistry & Engineering **6**, 147 (2021).
[25] L. Zeng, Y. Jiao, W. Yan, Y. Wu, S. Wang, P. Wang, D. Wang, Q. Yang, J. Wang, H. Zhang, and A. Lei, Nature Synthesis **2**, 172 (2023).
[26] T. Hibino, K. Kobayashi, M. Nagao, D. Zhou, S. Chen, and Y. Yamamoto, ACS Catalysis **13**, 8890 (2023).
[27] L. Zeng, Q. Yang, J. Wang, X. Wang, P. Wang, S. Wang, S. Lv, S. Muhammad, Y. Liu, H. Yi, and A. Lei, Science **385**, 216 (2024).

TABLE 1: **General principles of AC-induced chemoselectivity.** Predicted modifications to chemoselectivity when switching from DC to AC. Note that for quasi-reversible processes, sine AC may exhibit a behaviour similar to square AC due to the presence of an effective threshold potential – see Fig. 6F.

Type of branching	**Expected changes to chemoselectivity**	
	DC to square AC	*DC to sine AC*
Products of different oxidation states	Favours over-oxidation/over-reduction	Favours under-oxidation/under-reduction
Products of different stoichiometries	Favours product of lower stoichiometry (e.g. dimerisation)	Favours product of higher stoichiometry (e.g. dissociation)

[28] S. Rodrigo, C. Um, J. C. Mixdorf, D. Gunasekera, H. M. Nguyen, and L. Luo, Organic Letters **22**, 6719 (2020).
[29] E. O. Bortnikov and S. N. Semenov, The Journal of Organic Chemistry **86**, 782 (2021).
[30] D. Wang, T. Jiang, H. Wan, Z. Chen, J. Qi, A. Yang, Z. Huang, Y. Yuan, and A. Lei, Angewandte Chemie International Edition **61**, e202201543 (2022).
[31] Y. Yuan, J.-C. Qi, D.-X. Wang, Z. Chen, H. Wan, J.-Y. Zhu, H. Yi, A. D. Chowdhury, and A. Lei, CCS Chemistry **4**, 2674 (2022).
[32] E. O. Bortnikov, B. S. Smith, D. M. Volochnyuk, and S. N. Semenov, Chemistry – A European Journal **29**, e202203825 (2023).
[33] B. Lee, H. Naito, M. Nagao, and T. Hibino, Angewandte Chemie International Edition **51**, 6961 (2012).
[34] D. E. Blanco, B. Lee, and M. A. Modestino, Proceedings of the National Academy of Sciences **116**, 17683 (2019).
[35] L. E. Sattler, C. J. Otten, and G. Hilt, Chemistry – A European Journal **26**, 3129 (2020).
[36] J. Fährmann and G. Hilt, Angewandte Chemie International Edition **60**, 20313 (2021).
[37] Y. Kawamata, K. Hayashi, E. Carlson, S. Shaji, D. Waldmann, B. J. Simmons, J. T. Edwards, C. W. Zapf, M. Saito, and P. S. Baran, Journal of the American Chemical Society **143**, 16580 (2021).
[38] K. Hayashi, J. Griffin, K. C. Harper, Y. Kawamata, and P. S. Baran, Journal of the American Chemical Society **144**, 5762 (2022).
[39] D. Gunasekera, J. P. Mahajan, Y. Wanzi, S. Rodrigo, W. Liu, T. Tan, and L. Luo, Journal of the American Chemical Society **144**, 9874 (2022).
[40] N. Behera, D. Gunasekera, J. P. Mahajan, J. Frimpong, Z.-F. Liu, and L. Luo, Faraday Discussions **247**, 45 (2023).
[41] Y. Hioki, M. Costantini, J. Griffin, K. C. Harper, M. P. Merini, B. Nissl, Y. Kawamata, and P. S. Baran, Science **380**, 81 (2023).
[42] M. He, Y. Wu, R. Li, Y. Wang, C. Liu, and B. Zhang, Nature Communications **14**, 5088 (2023).
[43] A. F. Garrido-Castro, Y. Hioki, Y. Kusumoto, K. Hayashi, J. Griffin, K. C. Harper, Y. Kawamata, and P. S. Baran, Angewandte Chemie International Edition **62**, e202309157 (2023).
[44] S. Rodrigo, A. Hazra, J. P. Mahajan, H. M. Nguyen, and L. Luo, Journal of the American Chemical Society **145**, 21851 (2023).
[45] A. E. Remick and H. W. Mccormick, Journal of The Electrochemical Society **102**, 534 (1955).
[46] A. E. Remick and R. A. Marcus, Journal of The Electrochemical Society **109**, 628 (1962).
[47] D. D. Bump and A. E. Remick, Journal of The Electrochemical Society **111**, 981 (1964).
[48] M. Fleischmann, J. R. Mansfield, H. R. Thirsk, H. G. E. Wilson, and L. Wynne-Jones, Electrochimica Acta **12**, 967 (1967).
[49] A. M. Pesco and H. Y. Cheh, Journal of The Electrochemical Society **131**, 2259 (1984).
[50] C. G. Bell, C. A. Anastassiou, D. O'Hare, K. H. Parker, and J. H. Siggers, Electrochimica Acta **56**, 6131 (2011).
[51] C. G. Bell, C. A. Anastassiou, D. O'Hare, K. H. Parker, and J. H. Siggers, Electrochimica Acta **56**, 8492 (2011).
[52] P. S. Fedkiw and W. D. Scott, Journal of The Electrochemical Society **131**, 1304 (1984).
[53] T. R. Nolen and P. S. Fedkiw, Journal of The Electrochemical Society **137**, 2726 (1990).
[54] J. C. Smeltzer and P. S. Fedkiw, Journal of The Electrochemical Society **139**, 1358 (1992).
[55] J. C. Smeltzer and P. S. Fedkiw, Journal of The Electrochemical Society **139**, 1366 (1992).
[56] R. Bakshi and P. S. Fedkiw, Journal of Applied Electrochemistry **23**, 715 (1993).
[57] J. E. Nutting, J. B. Gerken, A. G. Stamoulis, D. L. Bruns, and S. S. Stahl, The Journal of Organic Chemistry **86**, 15875 (2021).
[58] More rigorously, E°_{ξ} represents the formal potential, which accounts for non-unity activity coefficients, together with contributions from the open-circuit potential.
[59] Strictly speaking, $E\,(t)$ represents the overpotential because we set $E = 0$ in the absence of an applied voltage.
[60] A. J. Bard, L. R. Faulkner, and H. S. White, *Electrochemical Methods: Fundamentals and Applications*, 3rd ed. (John Wiley & Sons, 2022).
[61] This may be observed from the Nernst relation which, for $n_1 = 1$, $n_2 = 2$ and $m_1 = m_2 = 1$, yields $E^{\circ}_1 - E^{\circ}_2 = (RT/F)\ln\left(\sqrt{c^*_{\mathrm{Re}}c^*_{\mathrm{Ox},2}}/c^*_{\mathrm{Ox},1}\right)$. Reducing $E^{\circ}_1 - E^{\circ}_2$ results in a higher $c^*_{\mathrm{Ox},1}$ value for fixed $c^*_{\mathrm{Ox},2}$ and c^*_{Re} values.
[62] P. H. Rieger, *Electrochemistry*, 2nd ed. (Springer Science & Business Media, 1994).
[63] M. A. Ardagh, O. A. Abdelrahman, and P. J. Dauenhauer, ACS Catalysis **9**, 6929 (2019).
[64] M. A. Ardagh, T. Birol, Q. Zhang, O. A. Abdelrahman, and P. J. Dauenhauer, Catalysis Science & Technology **9**, 5058 (2019).
[65] E. Cortés, L. V. Besteiro, A. Alabastri, A. Baldi, G. Tagliabue, A. Demetriadou, and P. Narang, ACS Nano **14**, 16202 (2020).
[66] M. J. Hülsey, C. W. Lim, and N. Yan, Chemical Science **11**, 1456 (2020).
[67] R. C. DiDomenico and T. Hanrath, ACS Energy Letters **7**, 292 (2021).
[68] A. Baldi and S. H. Askes, ACS Catalysis **13**, 3419 (2023).

[69] R. C. DiDomenico, K. Levine, C. Bundschu, L. Reimanis, T. Arias, and T. Hanrath, ACS Catalysis **14**, 785 (2024).
[70] S. R. Gathmann, C. J. Bartel, L. C. Grabow, O. A. Abdelrahman, C. D. Frisbie, and P. J. Dauenhauer, ACS Energy Letters **9**, 2013 (2024).
[71] P. Jangid, S. Chaudhury, and A. Kolomeisky, The Journal of Physical Chemistry C **128**, 9077 (2024).
[72] M. Murphy, K. Noordhoek, S. Gathmann, P. Dauenhauer, and C. Bartel, Catalytic resonance theory: Forecasting the flow of programmable catalytic loops (2024).
[73] S. Borsley, J. M. Gallagher, D. A. Leigh, and B. M. Roberts, Nature Reviews Chemistry **8**, 8 (2024).
[74] S. Borsley, D. A. Leigh, and B. M. Roberts, Angewandte Chemie International Edition **63**, e202400495 (2024).
[75] B. Kumar, J. P. Brian, V. Atla, S. Kumari, K. A. Bertram, R. T. White, and J. M. Spurgeon, ACS Catalysis **6**, 4739 (2016).
[76] Y. Liu, H. Jiang, and Z. Hou, Angewandte Chemie **133**, 11233 (2021).
[77] J. Wu, Chemical Reviews **122**, 10821 (2022).
[78] S. Gorthy, S. Verma, N. Sinha, S. Shetty, H. Nguyen, and M. Neurock, ACS Catalysis **13**, 12924 (2023).
[79] X. Zhu, J. Huang, and M. Eikerling, Hierarchical modeling of the local reaction environment in electrocatalysis (2024).
[80] E. J. Rudd and B. E. Conway, Transactions of the Faraday Society **67**, 440 (1971).
[81] P. Hu, B. K. Peters, C. A. Malapit, J. C. Vantourout, P. Wang, J. Li, L. Mele, P.-G. Echeverria, S. D. Minteer, and P. S. Baran, Journal of the American Chemical Society **142**, 20979 (2020).
[82] S. K. Bharti and R. Roy, TrAC Trends in Analytical Chemistry **35**, 5 (2012).
[83] G. F. Pauli, T. Godecke, B. U. Jaki, and D. C. Lankin, Journal of Natural Products **75**, 834 (2012).
[84] Q. Wan, K. Chen, X. Dong, X. Ruan, H. Yi, and S. Chen, Angewandte Chemie **135**, e202306460 (2023).